Biosensors and Bioelectronics 24 (2009) 2465–2469

Contents lists available at ScienceDirect

Biosensors and Bioelectronics

journal homepage: www.elsevier.com/locate/bios

WO_3 nanostructures facilitate electron transfer of enzyme: Application to detection of H_2O_2 with high selectivity

Zifeng Deng[a], Yichun Gong[a], Yongping Luo[a], Yang Tian[a,b,*]

[a] Department of Chemistry, Tongji University, Siping Road 1239, Shanghai 200092, PR China
[b] State Key Laboratory for Chemo/Biosensing and Chemometrics, College of Chemistry and Chemical Engineering, Hunan University, Changsha, PR China

ARTICLE INFO

Article history:
Received 23 October 2008
Received in revised form 15 December 2008
Accepted 17 December 2008
Available online 6 January 2009

Keywords:
Biosensor
Hydrogen peroxide (H_2O_2)
WO_3 nanostructures
Direct electron transfer
Enzyme

ABSTRACT

The WO_3 nanoparticles film is first employed as a support matrix for confining cytochrome *c* (cyt. *c*), an excellent model for studying electron transfer between the redox enzymes and the electrode. The surface pK_a of nanostructured WO_3 film is estimated to be ~2.74 using electrochemical method. The present WO_3 surface with negative charge at the neutral solution is very benefit for the adsorption of cyt. *c* with positive charge and facilitates electron transfer of cyt. *c*. As a result, direct and fast electron transfer of cyt. *c* is realized at the nanostructured WO_3 surface with the redox formal potential ($E^{0\prime}$) of -133.5 ± 1.7 mV ($n = 4$) versus Ag/AgCl and heterogeneous electron transfer rate constant of $5.57 \pm 0.54\ s^{-1}$. Experimental data indicate that cyt. *c* is stably confined onto the WO_3 nanoparticles film, possibly due to the electrostatic interaction between WO_3 nanostructures and cyt. *c*, and processes its enzymatic activity toward H_2O_2. Based on these results, the third-generation biosensor for H_2O_2 is developed with high selectivity, free from not only common anodic interferences like ascorbic acid, uric acid, 3,4-dihydroxyphenylacetic acid, and so on, but also cathodic interference—O_2. The remarkable analytical advantages, as well as the characteristic of WO_3 nanoparticles film such as biocompatibility, low-cost, and facile to miniature give a strong basis for continuous, on-line detection of H_2O_2 under pathophysiological conditions.

1. Introduction

H_2O_2—the most stable reactive oxygen species (ROS), which including superoxide anion ($O_2^{\bullet -}$), hydrogen peroxide (H_2O_2), and hydroxyl radical ($^{\bullet}OH$) has gained increasing attentions in a variety of research fields, because they are considered the mediators of the biochemistry of cellular pathology and may be involved in the etiology of aging and progressive neurodegenerative diseases, such as Parkinson's disease (Halliwell and Gutteridge, 1984; Hall and Braughler, 1989; Maruyama et al., 1995; Henzler and Steudle, 2000). H_2O_2 is also one of the productions of $O_2^{\bullet -}$ dismutation from superoxide dismutase (SOD) (McCord and Fridovich, 1969), and forms $^{\bullet}OH$ in the presence of transition metals such as iron and copper (Fenton reaction) (Theruvathu et al., 2001). As a consequence, the physiological levels of H_2O_2 are closely associated with the degradation and formation of reactive free radials, such as $O_2^{\bullet -}$ and $^{\bullet}OH$ (Mao et al., 2002). Therefore, a selective and sensitive method for reliable and durable determination of H_2O_2 is great essential and very useful for gaining a full understanding of the role that H_2O_2 and ROS play in pathology and physiology, and the relationship between H_2O_2 and environmental stresses and lipid peroxidation.

Over the past years, a number of strategies, such as titrimetry, spectrophotometry, chemiluminescence, and electrochemical methods have been developed to detect H_2O_2 (Shankaran et al., 2003; De Mattos et al., 2003; Garjonyte and Malinauskas, 1999; Sotomayor et al., 2003). Electrochemical approaches have been gained increasing attentions for the determination of H_2O_2 due to their direct, real-time measurements, and capability for practical applications (Gu et al., 2001; Lei et al., 2003; Tatsuma et al., 2001; Dong and Li, 1997; Miah and Ohsaka, 2006; Tatsuma and Watanabe, 1991; Tatsuma et al., 1994). Mostly, the third-generation biosensors based on direct electron transfer of enzymes and proteins have paved an elegant way to detect H_2O_2 due to excellent selectivity and high sensitivity, in which cytochrome *c* (cyt. *c*) (Zhang, 2008; Xiang et al., 2008; Jiang et al., 2006; Wang et al., 2002; Zhou et al., 2008; Liu et al., 2007), horseradish peroxidase (HRP) (Mao and Yamamoto, 2000; Ferapontova and Gorton, 2002; Karyakin et al., 2000; Kenausis et al., 1997), hemoglobin (Hb) (Liu et al., 2004; Shi et al., 2007; Sun et al., 2007; Lu et al., 2006a; Song et al., 1995), and myoglobin (Mb) (Holt and Cotton, 1989; Yang et al., 1993) have been widely employed. For this purpose, an amount of efforts have been paid on direct electron transfer of enzymes. Cyt. *c* is an excellent

* Corresponding author at: Department of Chemistry, Tongji University, Siping Road 1239, Shanghai 200092, PR China. Tel.: +86 21 65987075; fax: +86 21 65982287.
E-mail address: yangtian@mail.tongji.edu.cn (Y. Tian).

0956-5663/$ – see front matter © 2008 Elsevier B.V. All rights reserved.
doi:10.1016/j.bios.2008.12.037

model for studying the electron transfer of typical enzymes, since it has the special biological function of transferring electrons between membrane-bound enzyme complexes of cyt. *c* reductase and cyt. *c* oxidase. In addition, in the view of further applications, cyt. *c*-based H_2O_2 biosensor is capable of avoiding the interference of O_2 under a reasonable applied potential, since cyt. *c* is not a specific protein for O_2, unlike Hb and Mb—the carriers of O_2 in biological system. Therefore, in the past couple of decades, numerous applications of chemically or non-chemically modified methods to direct electron transfer of cyt. *c* have been exploited (Eddows and Hill, 1977; Eddows and Hill, 1979; Oliver et al., 1988; Taniguchi et al., 1984; Jiang et al., 2005; Yu and Ju, 2002; Wang and Wang, 2004).

With the development of nanomaterials, nanostructured semiconductors like TiO_2 and ZnO were reported useful for promoting electron transfer of heme proteins, and consequently for developing biosensors (Zheng et al., 2008; Liu et al., 2005; Zhang et al., 2004, 2007; Xiao et al., 2007; Lu et al., 2006b; Lin and Chen, 2006; Zhao et al., 2006; Deng et al., 2008). However, to the best of our knowledge, few papers were concerned with the direct electron transfer of cyt. *c* at WO_3 nanostructures (Feng et al., 2006). In the present work, it is the first time that direct electron transfer of cyt. *c* was achieved at WO_3 nanostructures with formal potential of -109.0 ± 1.7 mV versus Ag|AgCl, without any mediators or promoters. A combination of direct electrochemistry of cyt. *c* at the nanostructured WO_3 surface and enzymatic catalytic activity of cyt. *c* toward H_2O_2 paved a way for constructing a third-generation H_2O_2 biosensor with high selectivity. Besides this advantage, the present third-generation H_2O_2 biosensor exhibited broad dynamic linear range, low-detection limit, and quick response time.

2. Experimental

2.1. Reagents and materials

Horse heart cyt. *c* (MW 13,000) was obtained from Sigma and used without further purification. Other reagents were of analytical grade and used as received. ITO-coated glass plates with a square resistance of $\sim 10\ \Omega\ cm^{-2}$ were obtained from Shenzhen Nanbo Display Technology Co. Ltd. (Shenzhen, China). All the solutions were prepared with Milli-Q water and were deaerated with high-purity nitrogen before experiments. All electrochemical experiments were carried out at room temperature.

2.2. Fabrication and modification of nanostructured WO_3 film

ITO-coated glass plates were thoroughly cleaned by sonication for 30 min in the following solvents successively: soapy water, neat ethanol, 1 M NaOH and water. The WO_3 nanoparticles film was prepared by spin-coating method, using the sol mixed with WO_3 powder (20–50 nm) and deionized water under sonicating for 2 h, followed by annealed at 500 °C for 1 h under air atmosphere. The nanostructured WO_3 film was modified with cyt. *c* by immersing the WO_3 film into PBS (pH 7.2) of cyt. *c* (0.2 mM) for about 0.5–3 h at 3 °C in refrigerator. Hereafter, cyt. *c* modified-nanostructured WO_3 electrode will be referred as WO_3/cyt. *c*.

2.3. Apparatus and measurements

A CHI 660 and CHI 832 electrochemical work stations (CH Instruments) were employed in all electrochemical measurements, which were carried out with a conventional two compartment three-electrode electrochemical cell. The reference electrode was a KCl-saturated Ag|AgCl electrode, while the auxiliary electrode was a platinum wire. SEM images were taken by a Quanta 200 FEG (FEI Company). XRD pattern was obtained by a D/max2550VB3+/PC X-ray diffractormeter using Cu (40 kV, 100 mA).

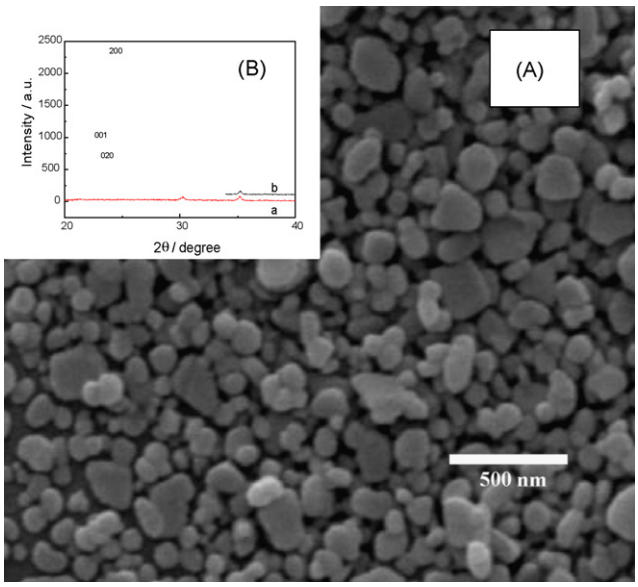

Fig. 1. (A) SEM image of WO_3 nanoparticles film. The bar corresponds to 500 nm; (B) X-ray diffraction patterns of ITO (a) and the WO_3 nanoparticles film (b).

3. Results and discussion

3.1. Surface properties of the nanostructured WO_3 film

A WO_3 nanoparticles film was characterized by scanning electron microscopy (SEM) as shown in Fig. 1(A). From the SEM image, we can see that the nanoparticles of WO_3 are typically 100 nm in diameter. The WO_3 nanoparticles film is porous and almost homogenous. The crystalline orientation of nanostructured WO_3 film was investigated by recording the X-ray diffraction (XRD) pattern. The diffraction peaks of ITO (a) and the WO_3 nanostructured film (b) are shown in Fig. 1(B). The pronounced peaks located at 23.125, 23.648, and 24.262, correspond to (0 0 1), (0 2 0), and (2 0 0) facets of WO_3, respectively (JCPDS card no. 20-1323).

The surface pK_a of the present WO_3 nanoparticles film was determined according to electrochemical method (Zhao et al., 1999), and calculated to be ~2.74. This result indicates that the nanostructured WO_3 surface shows negative charge at the neutral solution (pH 7.2). To further characterize electrochemical properties of the nanostructured WO_3 surface, cyclic voltammetry of an electron transfer indicator like $Fe(CN)_6^{3-/4-}$ was studied at the WO_3 nanoparticles electrode. As depicted in Fig. 2(A), at the WO_3 nanoparticles film, a severe decrease in the redox peak and a great widening of the peak-to-peak separation (ΔE_p) was observed, which may be ascribed to the electrostatic repulsion between $Fe(CN)_6^{3-}$ or $Fe(CN)_6^{4-}$ anion and the negatively charged nanostrucuted WO_3 surface. This observation was further confirmed by electrochemical impedance spectroscopy (EIS), as demonstrated in Fig. 2(B). The charge transfer resistance (R_{ct}) of $Fe(CN)_6^{3-/4-}$ redox couple is near 50 Ω at ITO substrate, but it increases to ~400 Ω at the nanostructured WO_3 surface (Fig. 2(B)b). The increase in the charge transfer resistance at the TiO_2 film, not the resistance of film (R_{film}) suggests again that the negatively charged WO_3 nanoparticles surface inhibits the electron transfer of $Fe(CN)_6^{3-}$ and/or $Fe(CN)_6^{4-}$ anion with same negative charge due to the electrostatic repulsion. On the other hand, at pH 7.2, cyt. *c* with p*I* = 9.5 has a net positive charge. As a result, the nanostructured WO_3 surface with negative charge may be very benefit for the adsorption of cyt. *c* due to the electrostatic interaction and subsequently facilitate the electron transfer of cyt. *c*.

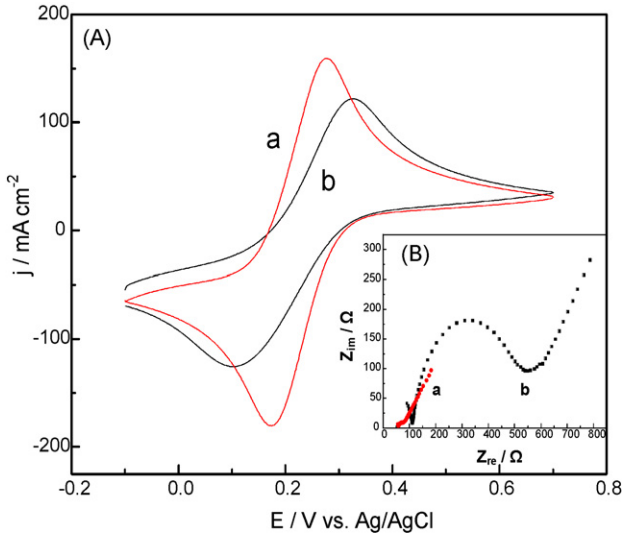

Fig. 2. (A) Cyclic voltammograms (CVs) obtained at ITO (a) and the nanostructured WO_3 surface (b) in 0.1 M KCl solution containing 1 mM $[Fe(CN)_6]^{3-/4-}$. Potential scan rate: 100 mV s^{-1}; (B) Nyquist plots of $[Fe(CN)_6]^{3-/4-}$ obtained at ITO (a) and the nanostructured WO_3 surface (b). EIS conditions: potential, 0.25 V; alternative voltage, 5 mV; frequency range, 0.1–105 Hz.

3.2. Electrochemical and spectroscopic characterization of cyt. c at the WO_3 nanoparticles film

As expected, a pair of redox peaks was observed at WO_3/cyt. *c* surface (b), while only charge current was obtained at WO_3 nanoneedles surface (a) in 25 mM PBS (pH 7.2) containing no cyt. *c* (Fig. 3(A)). The formal potential ($E^{0\prime} = (E_{p,a} + E_{p,c})/2$) of cyt. *c* obtained at WO_3 nanoparticles film is estimated to be -133.5 ± 1.7 mV ($n = 4$) versus Ag/AgCl.

CVs of WO_3/cyt. *c* electrode at various scan rates were also obtained in 25 mM fresh buffer solution containing no cyt. *c* (Fig. 4(A)). Both the anodic and cathodic peak currents (I_p^a and I_p^c) vary linearly with potential scan rate (v) in the range of 10–400 mV s^{-1}, as demonstrated in Fig. 4(B). In addition, the CVs remained essentially unchanged on consecutive potential scanning up to 1000 cycles at sweep rate of 20 mV s^{-1}, indicating that cyt. *c* was stably immobilized on the nanostructured WO_3 film. According to Laviron's procedure (Laviron, 1979), the relevant kinetic parameters of the electrode reaction, i.e. the rate constant of the electrochemical process (k_s) and cathodic transfer coefficients (α_c), were estimated: $k_s = 5.57 \pm 0.54$ s^{-1}, $\alpha_c = 0.42 \pm 0.02$ ($n = 4$) at the nanostructured WO_3 surface. It reveals that the direct electron transfer of cyt. *c* is strikingly enhanced at the WO_3 nanoparticles surface.

The adsorbed behavior of cyt. *c* was also confirmed by EIS. Fig. 3(B) shows Nyquist plots obtained at bare WO_3 nanoparticles film and WO_3/cyt. *c* electrode in 0.1 M KCl solution containing 1 mM $[Fe(CN)_6]^{3-/4-}$. The charge transfer resistance (R_{ct}) of $Fe(CN)_6^{3-/4-}$ redox couple is about 500 Ω at WO_3 nanoparticles film (a), but it increases to 1.1 KΩ after cyt. *c* was adsorped on the nanostructured WO_3 surface as shown in Fig. 3(B)b. These data suggested that cyt. *c* adsorbed onto the nanostructured WO_3 surface might inhibit the electrochemical communication between the electron transfer indicator—$Fe(CN)_6^{3-/4-}$ and the WO_3 nanoparticles electrode, resulting in the great increase of R_{ct} of $Fe(CN)_6^{3-/4-}$ redox couple. The equivalent circuit for an electrode undergoing heterogeneous electron transfer is usually described on the basis of the model by Randles as shown in Fig. 3. The circuit includes the ohmic resistance (R_s) of the electrolyte solution, Warburg impedance (Z_w), resulting from the diffusion of ions to the interface from the bulk of the electrolyte, double-layer capacitance (C_{dl}) and electron transfer

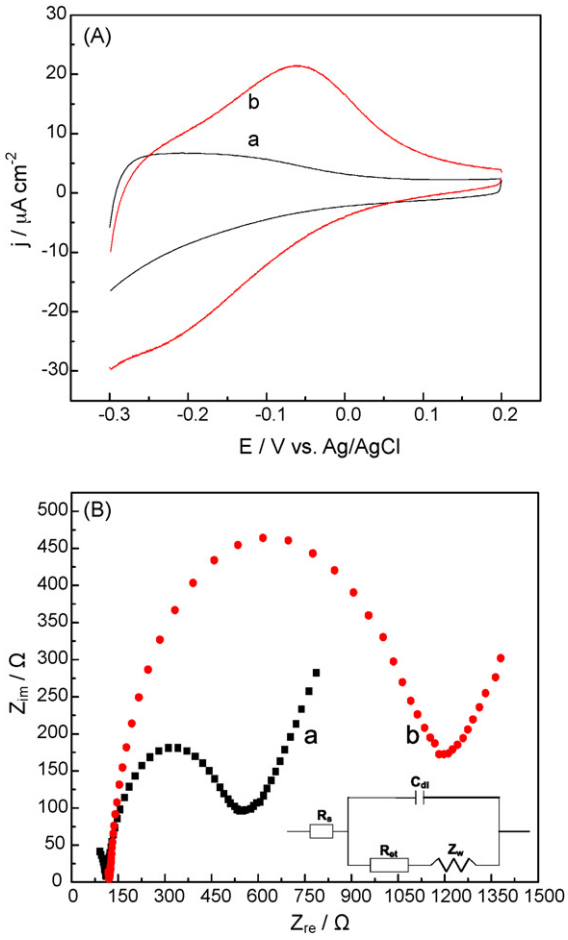

Fig. 3. (A) CVs obtained at (a) bare WO_3 nanoparticles film and (b) WO_3/cyt. *c* film in 25 mM PBS (pH 7.2). Potential scan rate: 100 mV s^{-1}; (B) Nyquist plots obtained at (a) bare WO_3 nanoparticles film and (b) WO_3/cyt. *c* electrode in 0.1 M KCl solution containing 1 mM $[Fe(CN)_6]^{3-/4-}$. EIS conditions: potential, 0.25 V; alternative voltage, 5 mV; frequency range, 0.1–105 Hz.

resistance (R_{et}). We use this equivalent circuit to fit the impedance spectroscopy and determine C_{dl} and R_{et}.

As described above, direct electron transfer of cyt. *c* was facilitated at the nanostructured WO_3 surface and electrochemical result

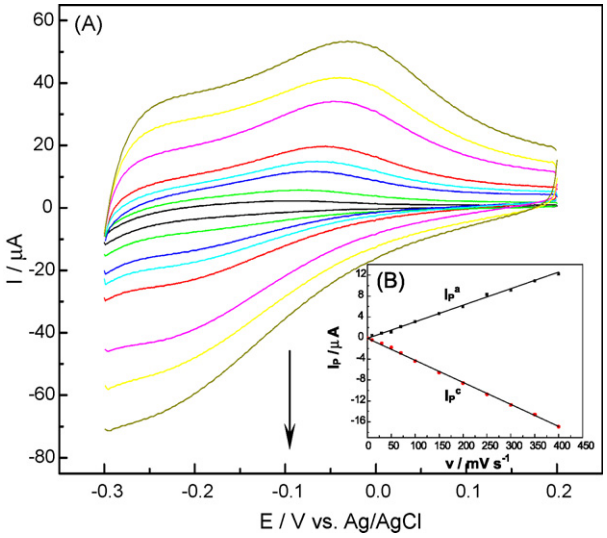

Fig. 4. (A) CVs obtained at WO_3/cyt. *c* film in 25 mM PBS (pH 7.2) with different scan rates: 10, 30, 50, 70, 100, 200, 300, and 400 mV s^{-1}; (B) relationship between anodic and cathodic peak currents of WO_3/cyt. *c* film and potential scan rate.

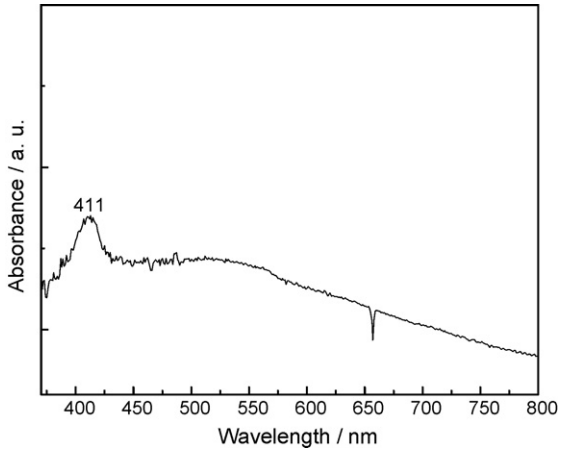

Fig. 5. UV–vis absorption spectrum of cyt. *c* confined on the WO_3 nanoparticles film.

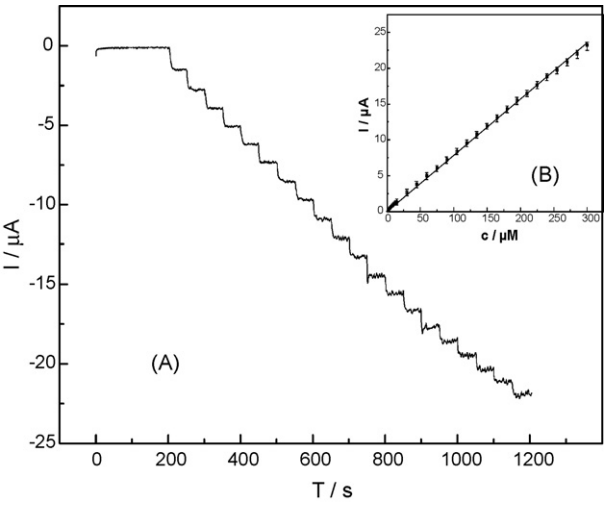

Fig. 6. (A) Typical amperometric responses of WO_3/cyt. *c* to successive additions of 15 μM H_2O_2 at applied potentials of −0.1 V vs. Ag/AgCl in 25 mM PBS (pH 7.2); (B) calibration plot of steady-state currents again concentrations of H_2O_2.

studies demonstrated that cyt. *c* was stably confined on the WO_3 nanoparticles film. Therefore, it is desirable to clarify whether cyt. *c* retains its inherent activity for H_2O_2 after adsorped on the WO_3 nanostructures. The Soret band of heme protein is usually an indicator of the microenvironment where heme center locates. The peak will be diminished if the protein is denaturated (Nassar et al., 1995; Wang et al., 2005). Fig. 5 shows UV–vis absorption spectrum of cyt. *c* confined on the optical transparent WO_3 nanoparticles surface. The band for cyt. *c* adsorbed on the nanostructured WO_3 film is located at 411 nm, just a 1-nm blue shift compared with that of native cyt. *c* solution (410 nm, data not shown). This observation revealed that cyt. *c* almost processed its intrinsic activity after adsorbed on the WO_3 nanoparticls film.

3.3. Analytical performance of the H_2O_2 biosensor

The direct electron transfer of cyt. *c* was enhanced at the WO_3 nanoparticles surface, and cyt. *c* immobilized on the nanostructured WO_3 film almost processed the enzymatic activity. These results provided a platform for constructing the third-generation biosensor for H_2O_2 because the heme has been well documented as the active site for the catalysis to the reduction of H_2O_2.

As well known, the sensitivity of electrochemical biosensors is strongly dependent on the applied potential. The cathodic current intensity of H_2O_2 obtained at WO_3/cyt. *c* film increased with the negative shift of the operating potentials (data not shown). This observation indicates that more negative the operating potential, higher sensitivity the H_2O_2 biosensor shows. Meanwhile, the selectivity of electrochemical biosensors is also potential-dependent. The coexisting biological compounds, not only anodic interferences such as AA, UA, and so on, but also cathodic interference—O_2 may interfere with the electrochemical determinations of H_2O_2. Eight kinds of interferences including UA, AA, DA, DOPAC, NO_3^-, NO_2^-, SO_3^{2-}, and O_2 were examined. At the optimized potential of −0.1 V, both anodic and cathodic potential interferences were negligible (<2.5%). Therefore, for fulfill both selectivity and sensitivity of the present biosensor, −0.1 V (versus Ag/AgCl) was selected as the optimized operating potential. The sensitivity of the present biosensor at this applied potential was estimated to be 63.51 mA cm^{-2} M^{-1}.

Amperometric responses of WO_3/cyt. *c*, to successive concentration changes of H_2O_2 were conducted at the optimized potential of −0.1 V, and the corresponding current–time responses are shown in Fig. 6(A). Well-defined steady-state current responses were obtained and the currents increased stepwise with successive additions of H_2O_2. The calibration plot is depicted in Fig. 6(B). Besides high selectivity, the present H_2O_2 biosensor shows excellent analytical performance, for instance, wide linear detection range from 3×10^{-7} to 3×10^{-4} M, low-detection limit (2.4×10^{-7} M), and short response time of 5 s. The performance of the WO_3/cyt. *c* biosensor developed in this study was compared with other biosensors as shown in Table S1, showing that our proposed biosensor shows excellent performance, such as low-detection limit and wide linear detection range. This remarkable analytical performance fulfills the requirement of in vivo or on line tracking of H_2O_2 concentration.

For the stability test, the 100 continuous cyclic scans was carried out in the potential range from −0.3 to 0.2 V with a 100 mV s^{-1} scan rate, only 5% decrease of the initial response is observed. On the other hand, the storage stability of the proposed biosensor was also studied. When not in use, the electrode was stored in the phosphate buffer at 4 °C in a refrigerator. The cathodic responses for H_2O_2 were found to be constant for at least 30 days. In addition, we have found that the deviation of the current responses of 10 sensors prepared with the same method did not exceed 3% (RSD).

4. Conclusions

Direct electron transfer of cyt. *c* was developed at the nanostructured WO_3 surface with negative charge. The formal potential was estimated to be -133.5 ± 1.7 mV (versus Ag/AgCl), and the electrochemical process was reversible with heterogeneous electron transfer rate constant of 5.57 ± 0.54 s^{-1}. Experimental results revealed that cyt. *c* was stably confined onto the nanostructured WO_3 film, possibly due to the electrostatic interaction, and spectroscopic data suggested that cyt. *c* held its inherent enzymatic activity. As a consequence, a third-generation H_2O_2 biosensor was achieved with high selectivity, free from not only the anodic interferences, such as UA, AA, DOPAC, and so on, but also the cathodic interference—O_2. Besides this advantage, the present H_2O_2 biosensor also showed broad dynamic linear range, low-detection limit, and quick response time. The striking analytical characteristics, together with the intrinsic properties of WO_3 nanostructures, such as biocompability, easy to prepare, and facile of miniaturize, sufficiently offered an electrochemical approach to continuous, on-line detection of H_2O_2 under pathophysiological conditions. This work provided a methodology to enhance electron transfer of enzymes, especially the enzymes with high p*I* at the nanostructured WO_3 surface with negative charge, as well as on the basis of this platform to develop the third-generation biosensors with high-analytical performance.

Acknowledgements

This work was financially supported by Program for New Century Excellent Talents in University (NCET-06-0380) and the Scientific Research Foundation for the Returned Overseas Chinese Scholars from State Education Ministry, China, and Shanghai Pujiang Program (06PJ14090). Tongji University is also greatly acknowledged.

Appendix A. Supplementary data

Supplementary data associated with this article can be found, in the online version, at doi:10.1016/j.bios.2008.12.037.

References

De Mattos, I.L., Gorton, L., Ruzgas, T., 2003. Biosens. Bioelectron. 18, 193–200.
Deng, Z., Yin, X., Rui, Q., Liu, H., Tian, Y., 2008. Anal. Chem. 80, 5839–5846.
Dong, S., Li, J., 1997. Bioelectrochem. Bioenergy 42, 7–13.
Eddows, M.J., Hill, H.A.O., 1977. J. Chem. Soc. Chem. Commun. 21, 771–772.
Eddows, M.J., Hill, H.A.O., 1979. J. Am. Chem. Soc. 101, 4461–4464.
Feng, J., Xu, J., Chen, H., 2006. Electrochem. Commun. 8, 77–82.
Ferapontova, E., Gorton, L., 2002. Bioelectrochemistry 55, 83–87.
Garjonyte, R., Malinauskas, A., 1999. Sens. Actuat. B 56, 93–97.
Gu, H., Yu, A., Chen, H., 2001. J. Electroanal. Chem. 516, 119–126.
Hall, E.D., Braughler, J.M., 1989. Free Radic. Biol. Med. 6, 303–313.
Halliwell, B., Gutteridge, J.M.C., 1984. Biochem. J. 219, 1–14.
Henzler, T., Steudle, E., 2000. J. Exp. Bot. 51, 2053–2059.
Holt, R.E., Cotton, T.M., 1989. J. Am. Chem. Soc. 111, 2815–2821.
Jiang, X., Shang, L., Wang, Y., Dong, S., 2005. Biomacromolecules 6, 3030–3036.
Jiang, X., Zhang, L., Dong, S., 2006. Electrochem. Commun. 8, 1137–1141.
Karyakin, A.A., Karyakina, E.E., Gorton, L., 2000. Anal. Chem. 72, 1720–1723.
Kenausis, G., Chen, Q., Heller, A., 1997. Anal. Chem. 69, 1054–1060.
Laviron, E., 1979. J. Electroanal. Chem. 101, 19–28.
Lei, C., Hu, S., Shen, G., Yu, R., 2003. Talanta 59, 981–988.
Lin, K., Chen, S., 2006. Biosen. Bioelectron. 21, 1737–1745.
Liu, A., Wei, M., Honma, I., Zhou, H., 2005. Anal. Chem. 77, 8068–8077.
Liu, H., Rusling, J.F., Hu, N., 2004. Langmuir 20, 10700–10705.
Liu, H., Tian, Y., Xia, P., 2007. Langmuir 23, 9487–9494.
Lu, H., Yang, J., Rusling, J.F., Hu, N., 2006a. Electroanalysis 18, 379–390.
Lu, X., Hu, J., Yao, X., Li, J., 2006b. Biomacromolecules 7, 975–980.
Mao, L., Osbome, P.G., Yamamoto, K., Kato, T., 2002. Anal. Chem. 74, 3684–3689.
Mao, L., Yamamoto, K., 2000. Talanta 51, 187–195.
Maruyama, W., Dostert, P., Matsubara, K., Naoi, M., 1995. Free Radic. Biol. Med. 19, 67–75.
McCord, J.M., Fridovich, I., 1969. J. Biol. Chem. 244, 6049–6055.
Miah, M., Ohsaka, T., 2006. Anal. Chem. 78, 1200–1205.
Nassar, A.F., Willis, W.S., Rusling, J.F., 1995. Anal. Chem. 67, 2386–2392.
Oliver, B.N., Egekeze, J.O., Murray, R.W., 1988. J. Am. Chem. Soc. 110, 2321–2322.
Shankaran, D.R., Iimura, K.I., Kato, T., 2003. Sens. Actuat. B 96, 523–526.
Shi, G., Sun, Z., Liu, M., Zhang, L., Liu, Y., Qu, Y., Jin, L., 2007. Anal. Chem. 79, 3581–3588.
Song, M.I., Bier, F.F., Scheller, F.W., 1995. Bioelectrochem. Bioenergy 38, 419–422.
Sotomayor, M.D.P.T., Tanaka, A.A., Kubota, L.T., 2003. Electrochim. Acta 48, 855–865.
Sun, W., Gao, R., Jiao, K., 2007. J. Phys. Chem. B 111, 4560–4567.
Taniguchi, I., Iseki, M., Toyosawa, K., Yamaguchi, I., Yasukouchi, K., 1984. J. Electroanal. Chem. 164, 385–391.
Tatsuma, T., Ogawa, T., Sato, R., Oyama, N., 2001. J. Electroanal. Chem. 501, 180–185.
Tatsuma, T., Watanabe, T., 1991. Anal. Chem. 63, 1580–1585.
Tatsuma, T., Watanabe, T., Tatsuma, S., Watanabe, T., 1994. Anal. Chem. 66, 290–294.
Theruvathu, J.A., Aravindakumar, C.T., Flyunt, R., von Sonntag, J., von Sonntag, C., 2001. J. Am. Chem. Soc. 123, 9007–9014.
Wang, C., Yang, C., Song, Y., Gao, W., Xia, X., 2005. Adv. Funct. Mater. 15, 1269–1275.
Wang, J., Li, M., Shi, Z., Li, N., Gu, Z., 2002. Anal. Chem. 74, 1993–1997.
Wang, L., Wang, E., 2004. Electrochem. Commun. 6, 49–54.
Xiang, C., Zou, Y., Sun, L., Xu, F., 2008. Electrochem. Commun. 10, 38–41.
Xiao, P., Garcia, B.B., Guo, Q., Liu, D., Cao, G., 2007. Electrochem. Commun. 9, 2441–2447.
Yang, M., Chung, F.L., Thompson, M., 1993. Anal. Chem. 65, 3713–3716.
Yu, J., Ju, H., 2002. Anal. Chem. 74, 3579–3583.
Zhang, L., 2008. Biosen. Bioelectron. 23, 1610–1615.
Zhang, L., Zhang, Q., Li, J., 2007. Adv. Funct. Mater. 17, 1958–1965.
Zhang, Y., He, P., Hu, N., 2004. Electrochim. Acta 49, 1981–1988.
Zhao, G., Xu, J., Chen, H., 2006. Anal. Biochem. 350, 145–150.
Zhao, J., Luo, L., Yang, X., Wang, E., Dong, S., 1999. Electroanalysis 11, 1108–1111.
Zheng, W., Zheng, Y., Jin, K., Wang, N., 2008. Talanta 74, 1414–1419.
Zhou, Y., Zhi, J., Zou, Y., Zhang, W., Lee, S., 2008. Anal. Chem. 80, 4141–4146.